Revisiting behavior of monometallic catalysts in chemical vapor deposition synthesis of single-walled carbon nanotubes

Rong Xiang,*[1] Shigeo Maruyama*[1,2]

[1] *Department of Mechanical Engineering, The University of Tokyo, Tokyo 113-8656, Japan.*
[2] *Energy NanoEngineering Laboratory, National Institute of Advanced Industrial Science and Technology (AIST), Tsukuba 305-8564, Japan*

Abstract

Catalyst is essential for the controlled synthesis of single-walled carbon nanotube (SWNT) in chemical vapor deposition (CVD). However, it is difficult to observe these nano-sized particles in their original forms and in a statistical manner, which resulted in a vague understanding of the behaviors of these particles. We present a technique to solve this long-standing issue. The key is to have a MEMS fabricated suspended SiO_2 layer, which is thick enough to support catalyst deposition and nanotube growth but thin enough to allow electron beam to transit. On a 20 nm SiO_2 film, we confirm that catalyst can be observed at an atomic resolution, and the catalyst-SWNT junctions can also be routinely observed. As a demonstration of this technique, we revisited the behavior of mono-metallic catalyst through a systematic investigation on the size, chemical state, and crystal structure of particles before and after the high temperature CVD. The active catalyst are found to follow a tangential growth mode, while the inactive catalyst are divided into three mechanisms: size growth, metal loss, and inappropriate precipitation. The latter two mechanisms were not possible to observe by previous techniques.

*correspondence may be addressed: xiangrong@photon.t.u-tokyo.ac.jp (R. X.) and maruyama@photon.t.u-tokyo.ac.jp (S. M.)

1. Introduction

Single-walled carbon nanotube (SWNT), as the representative 1D nano-material, has attracted much attention in the past decades due to the outstanding properties and potential applications. To synthesize this unique 1D structure, a nano-size particle is usually needed. It serves as the nucleation site for carbon precipitation, and therefore is essential for the structure of product. [1]

Great efforts have been made on the exploration and optimization of catalyst. In 1996, the first report on CVD synthesis of SWNT employed pre-formed Mo particles as catalyst.[2] Soon later, in 1998, transition metals (in particular, Fe, Co, Ni) were proposed and confirmed to be more efficient.[3] They quickly became the most-used active sites for laboratorial and industrial scale SWNT productions. Different from transit metals, novel metals (Au, Pt, Pd, etc.) were traditionally inactive, but researchers found in 2006 that they can be activated to produce clean SWNTs with decent efficiency.[4] In the following years, semiconductor,[5] oxide,[6] and more recently intermetallic compound,[7] carbide,[8] were introduced as a new class of catalyst: solid catalyst. One major feature of these catalyst is their capability of producing SWNTs with selective conductance or chirality.[7-9]

Though great progresses have been achieved so far, previous explorations on catalyst were in most cases based on empirical studies, which resulted in a very vague understanding on the behaviors of these catalyst and the growth mechanism of SWNTs. One main reason behind is the absence of a technique to characterize nano-sized catalytic particles in a highly reliable manner. Transmission electron microscopy (TEM) is the most powerful and straightforward for visualizing catalyst, but the conventional method only sees a very small area. Furthermore the catalyst are usually not in their original forms, either sitting on different support (e.g. carbon or Si3N4 grid), or undergo very different environment (e.g. low growth pressure in an e-TEM condition).

In this contribution, we present an attempt to address this two-decade-standing issue. The key we propose is to have a MEMS fabricated suspended SiO_2 layer that is thick enough to support catalyst deposition and nanotube growth but thin enough to allow electron beam to transit (Figure 1a). In this scenario, the catalyst particles are prepared and CVD is performed directly on this Si/SiO_2 grid (Figure 1b), similar to conventional processes on Si/SiO_2 substrate. But the thin SiO_2 region enables a transfer-free characterization of the catalyst/SWNTs and minimize the information loss from CVD chamber to TEM column. Additionally, all images are taken from a bird view, in which many particles are present simultaneously. We believe this study can provide so far the most statistical and intrinsic information of the nano-size particles used for CVD synthesis of SWNTs. As an example, mono-metallic catalyst is systematically re-investigated and their behaviors in CVD synthesis are revisited. New understanding on the catalyst structure, catalyst-SWNT junction, and catalyst deactivation mechanism are illustrated.

2. Experimental

Monometallic catalyst is prepared onto the grid by sputtering. The nominal thickness is 0.3 nm in all cases. The catalyst in Fig. 2c&d is prepared by drop-casting a 50 µl catalyst solution (cobalt acetate in ethanol, 0.01mmol/L) directly on the grid. After catalyst deposition, the substrate is annealed in air at 400°C, followed by a reduction in a 40 kPa Ar diluted H_2 (3%) atmosphere at 800°C for 10 min. After reduction, the grid is either taken out from the furnace for a TEM characterization or continued with a SWNT growth. SWNTs are grown in low pressure alcohol catalytic CVD (ACCVD) apparatus equipped with a dry rotatory pump.[10] The CVD temperature is 800°C for all cases in this study unless elsewhere stated, and pure ethanol is used as the carbon source without any carrier gas. Typically, after reduction, a flow of 450 sccm of ethanol is introduced into the chamber at a pressure of 1.3 kPa. In order to avoid the overgrowth of SWNTs that are too thick for TEM observations, the ethanol flow is kept for only 2 seconds. However, since there is a delay in refreshing the chamber atmosphere, the total exposure time for catalyst to ethanol is around several seconds. After growth, ethanol feeding is stopped and the sample is cooled down to room temperature in a flow of 50 sccm Ar diluted H_2 (3%). TEM images are obtained by using JEM-2000EX-II (JEOL Co. Ltd), JEM-2010F (JEOL Co., Ltd) and abbreviation corrected TEM ARM200 (JEOL Co., Ltd). All three TEMs are operated at 200 keV. Selected area electron diffraction (SAED) patterns are obtained by using JEM-2010F with a camera length of 60 cm at a parallel beam.

3. Results and discussion

3.1 Overview of imaging catalyst and SWNTs on SiO_2 film.

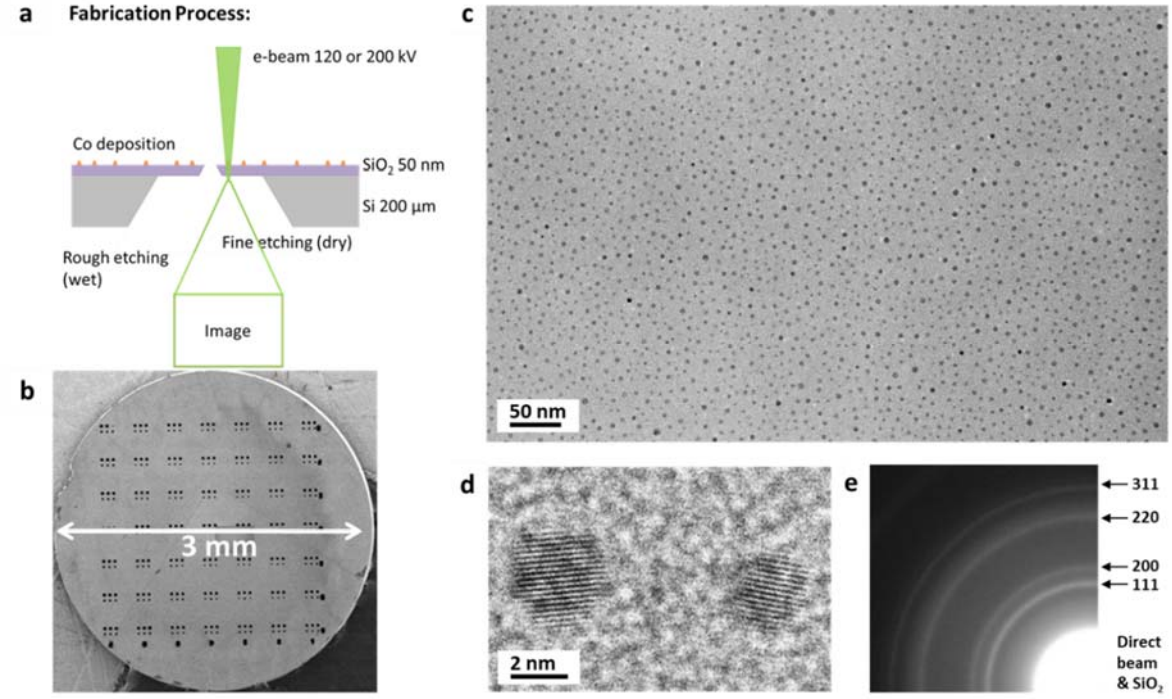

Figure 1 (a) a schematic and fabrication process of a MEMS fabricated Si/SiO_2 TEM grid; (b) SEM

image of the final 3 mm diameter product that fits a conventional TEM hold; representative (c) low-mag. and (d) high mag. TEM images of Co nano-particles sitting on a thin SiO_2 film; (e) a SAED pattern of Co catalyst obtained with an aperture diameter of 7 μm.

Figure 1a and b shows the typical structural and an SEM image of the Si/SiO_2 grid used in this study. The grid is fabricated by standard photolithography followed by wet and dry etching. A thin layer of SiO_2 (20-50 nm) is used as the supporting film for catalyst and serves as the observation window. This thin film and the whole grid is stable at high temperatures up to 1000°C. Therefore, after catalyst loading, the grid can be directly used for SWNT growth, which is similar to a standard Si/SiO_2 substrate (Fig. S1).

Figure 1c shows a representative low magnification TEM image of mono-metallic Co catalyst sitting on thin SiO_2 film. The catalyst are prepared by sputtering and therefore has a good uniformity over the entire grid. Even seeing through the SiO_2 film, one can clearly distinguish the strong contrast of nano-particles from the amorphous background. The lattice fringe of these catalyst can also been routinely observed by a conventional TEM (Fig. 1d). The size of particles distributes from 2-6 nm, with a mean diameter of ~3 nm. This value is slightly large for growth of SWNTs, which is consistent with many of previous empirical understandings that monometallic particles alone are usually not the most efficient. Some additional ingredients, e.g. Mo, Al, are needed to help disperse and prevent sintering of these catalyst at high temperatures.[11, 12] This process will be demonstrated and discussed in detail in the later section.

As catalyst can be visualized in a large area, selective area electronic diffraction (SAED) is a powerful way to determine the crystal structure of these particles. Inset of Figure 1e show a typical SAED pattern of monometallic Co catalyst. Surprisingly, the pattern unambiguously suggests that these Co particles have a dominant facet center cubic (fcc) structure, which is different from classic phase diagram that Co is hexagonal close packed (hcp) at the room temperature and transits to fcc only at a temperature above 700°C.[13] Though in contrast with almost all previous discussions (where Co were believed to be hcp),[14] this result is understandable because nano-particles tend to form simple fcc structures at reduced size.[15] The density of these catalyst in this case is estimated to be 8000 μm^{-2}, which is on the same order of magnitude as our previous measurement of a vertically aligned SWNT array.[16] This suggests our SAED pattern obtained from an area Φ 7 μm, contains roughly 300,000 particles, meaning very statistic information of catalyst particles are obtained. This is unique and a powerful feature for catalyst investigations.

High resolution images of these catalyst are consistent with the SAED assignment, where many particles shows a lattice fringe of 2.0 Å, which corresponds to the (111) plane of fcc Co. Most particles present characteristic features as single crystals, but twin- and poly-crystals are also occasionally observed for larger particles. While most catalyst are confirmed to be fcc metallic Co, oxide layer can be observed after the sample is exposed to air. In this case, overnight annealing in a

reduction atmosphere, and/or introducing trace amount of carbon at high temperatures help to keep the particles in metallic forms. One technical issue when obtaining high resolution images on this special grid is that SiO_2 is not conductive, which is major difference from conventional grid made of Cu and carbon. On SiO_2 film, it is critical to keep a low electron dose to obtain a stable image. With the reduced electron dose, lattice fringe and atomic resolution can be repeatedly obtained.

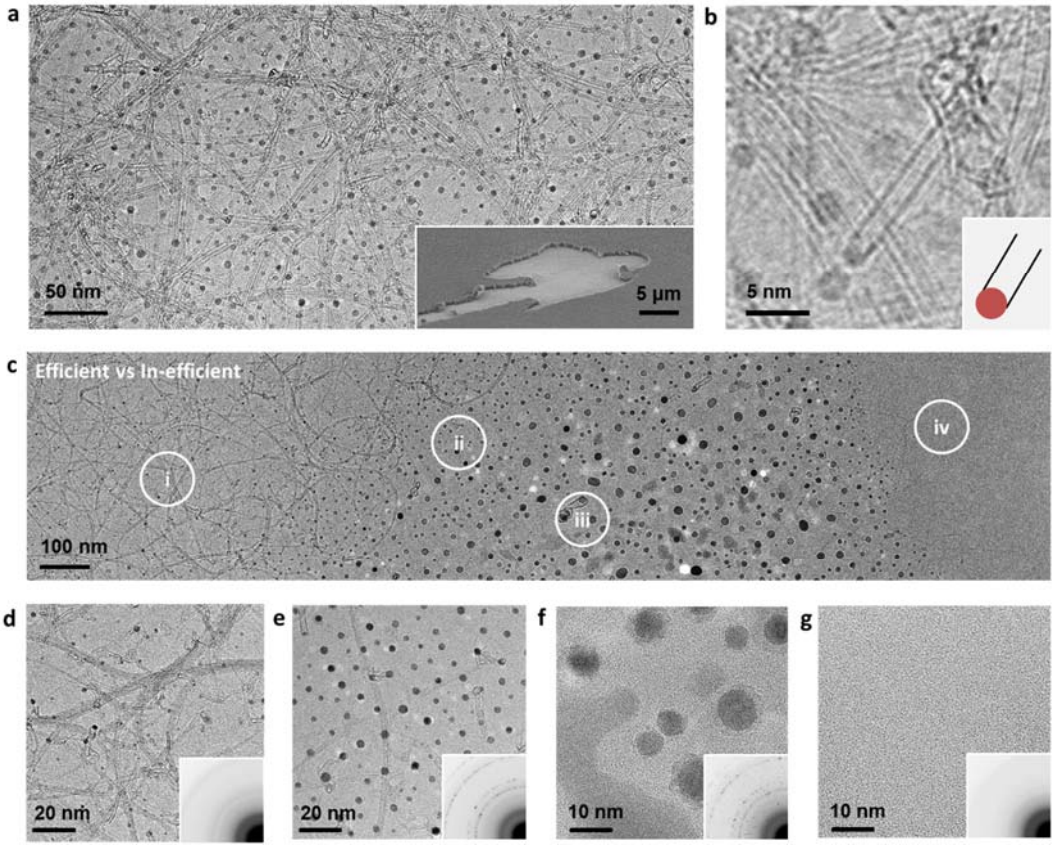

Figure 2 (a) (b) Representative TEM images of catalyst particles on SiO_2 grid after a short-time CVD: SWNTs are clearly observed in their original form, and the junction between a catalyst and a SWNT suggest a tangential growth mode; inset shows an SEM image of SWNTs grown on TEM grid. (c) TEM images of a region with gradient change of catalyst concentration, which reveal locally the difference between efficient and in-efficient catalyst. (d)-(g) enlarged images and SAED patterns (inset) corresponding to the locations (i)-(iv).

This Si/SiO_2 grid is stable at high temperatures so can be placed into a furnace for direct SWNT synthesis, as previously noted. Representative TEM images of the same grid after a several sec. CVD are shown in Fig. 2a. Single and bundled SWNTs are clearly observed on this SiO_2 film in their as-grown form. The growth behavior and growth rate on this TEM grid is similar to the case on standard Si/SiO_2 substrate. After longer CVD, even thicker SWNTs can be achieved (SEM shown as inset of Fig. 2a). But significantly different from conventional substrate growth, SWNTs in this

case can be directly characterized after CVD, no any post-transfer or sampling process are involved. If SWNTs are not too thick, catalyst can also be imaged. The enlarged image in Fig. 2b suggests the diameter of SWNT grown is almost the same as the catalyst particle. This confirms that SWNTs follow a tangential growth mode in this study.[17] However, this observation does not disapprove that monometallic catalyst may also follow a vertical mode, as CVD condition and other parameters (e.g. carbon solubility) may affect the growth mechanism.[18] Though more efforts are required, studying the junction between a catalyst and SWNT becomes possible by this approach.

When the catalyst is prepared with a gradient, the local difference between efficient and in-efficient areas can be identified. Figure 2c shows one example of SWNTs grown from wet-prepared catalyst. The aprox. 0.5 * 2 μm^2 area can be clearly classified as four regions: (i) efficient, (ii) less efficient, (iii) not efficient, (iv) reference. Figure 2d-g are the corresponding enlarged TEM images and SAED patterns of these four regions. Because the catalysts undergo an exact CVD environment (temperature, pressure, even local flow), this difference in efficiency is solely attributed to catalyst, that is, amount of metal precursor deposited in a local area. In region (i), small catalyst particles are formed and SWNT are efficiently produced (Figure 2d). However, in region (ii) where the amount slightly increase, most particles aggregate above 5 nm and the SWNT yield dramatically decreases (Figure 2e). Large diameter SWNTs and few walled CNTs appear. In region (iii) where the metal amount further increases, both the image and SAED patterns reveal the co-existence of Co metal and Co oxide (Figure 2f). This suggests the reduction is even not complete and explains the inefficiency. These differences were vaguely understood in previous batch-to-batch studies, but now can be clearly visualized by the current technique.

With this technique we systematically re-examined the size, density, chemical state and crystal structure of various monometallic catalyst before and after CVD, together with the yield, structure, and growth of mode of the produced SWNTs. The results are summarized and compared in Table 1. Overall, SWNTs are observed in TEM for all metals except W, but the SWNT yield varies largely from metal to metal (Figure 3a). Only Co and Ni produce Raman detectable amount of SWNTs, while other metals result in either short, or long but very sparse SWNTs. This is probably why they are concluded as “in-active” or at least “in-efficient” after previous characterizations by, e.g. Raman and/or SEM. However, the nature of the current technique allows to access many detailed information regarding the catalyst and in-depth understanding on their behaviors. According to the observations, we classify these less efficient catalysts into three different mechanisms and discuss separately in the next section.

3.2 Three different mechanism for in-efficient catalyst

Because the SiO_2 grid can be put into a furnace for SWNT growth and then taken out for a TEM re-check, imaging the exactly same location before and after CVD becomes possible. One

example is shown as Figure 3b, where the morphology of Ni catalyst before and after a short time (few sec.) CVD are compared (Fig. S2). It is straightforward from the images that an increase of particle diameter occurs after introducing the carbon source (ethanol). The original average particle size was less than 3 nm, but quickly changed to around 5 nm after the exposure to ethanol for a few seconds. Though a small number of 2-3 nm particles still remain, the overall efficiency drastically deteriorates. This explains the observations that Ni alone produces long but very sparse SWNTs. As a comparison, Co, the most efficient catalyst in this study, maintained its size after CVD, and yields much denser SWNTs. Also, the SAED patterns Figure 3c suggest Ni particles were partially oxidized before CVD but become pure metallic after CVD starts. This also reveals the ethanol CVD is a typical reduction process, even though ethanol is an oxygen-containing molecule. For a comparison, the histograms of the particle size distribution of Ni and Co are shown as Figure 3d and 3e, in which Co is able to maintain its size while Ni undergoes a clear particle coarsening.

Table 1 Summary of behavior of various monometallic catalyst before and after CVD

Element		Co	Ni	Fe	Cu	Pt	Pd	W
Bulk properties	Structure	hcp	fcc	Bcc	fcc	fcc	fcc	bcc
	m.p. (K)	1768	1728	1811	1357.77	2041.4	1828.05	3695
	b.p. (K)	3200	3003	3134	2835	4098 K	3236	6203
Particle size	Before CVD	2.6	2.8	6.0	4.6	2.3	2.3	2.9
	After CVD	2.8	5.1	7.7	5.9	2.4	2.7	n/a
number density (μm^{-2})	Before CVD	8E3	1.2E4	2E3	4.2E3	2.3E4	1.8E4	1.4E4
	After CVD	3.8E3	3.0E3	2E2	5.8E2	2.0E4	1.1E4	n/a
Oxidation	Before CVD	slight	medium	heavy	slight	metallic	metallic	metallic
	After CVD	metallic	metallic	metallic	metallic	metallic	metallic	n/a
Particle Structure	Before CVD	fcc	fcc	bcc	fcc	fcc	fcc	bcc
	After CVD	fcc	fcc	bcc	fcc	fcc	fcc	bcc
SWNT Growth	yield	◎	○	△	△	△	△	×
	diameter	1-3	2-5	2-5	2-5	~1	1-2	n/a
	length	long	long	long	media	Short	short	n/a
	density	high	low	low	low	Very high	Very high	n/a
	mode	tangential	tangential	vertical	both	tangential	tangential	n/a

However, we claim the size increase of Ni is carbon induced. In a control experiment, we kept Ni in a carbon-free reductive atmosphere for more than 60 mins (much longer than the time scale of a typical CVD process). After this long-time annealing, the particles are still in the similar size with as-reduced catalyst (the one in Figure 3b), which clearly evidences that the size change for Ni is dominantly caused by carbon induction. This behavior of Ni is also very different from Fe. (Fig. S3 & S4) In case of Fe, most particles were already in an inappropriate size (about 5-6 nm shown in Table 1) before CVD, therefore is intrinsically too large for an efficient growth of SWNTs. In this sense, we emphasize that for monometallic catalyst, Ni is one promising candidate for high efficient synthesis, as long as the carbon-induced size increase can be refrained, e.g., by lowering the carbon feeding speed, i.e. partial pressure of carbon source in the chamber.

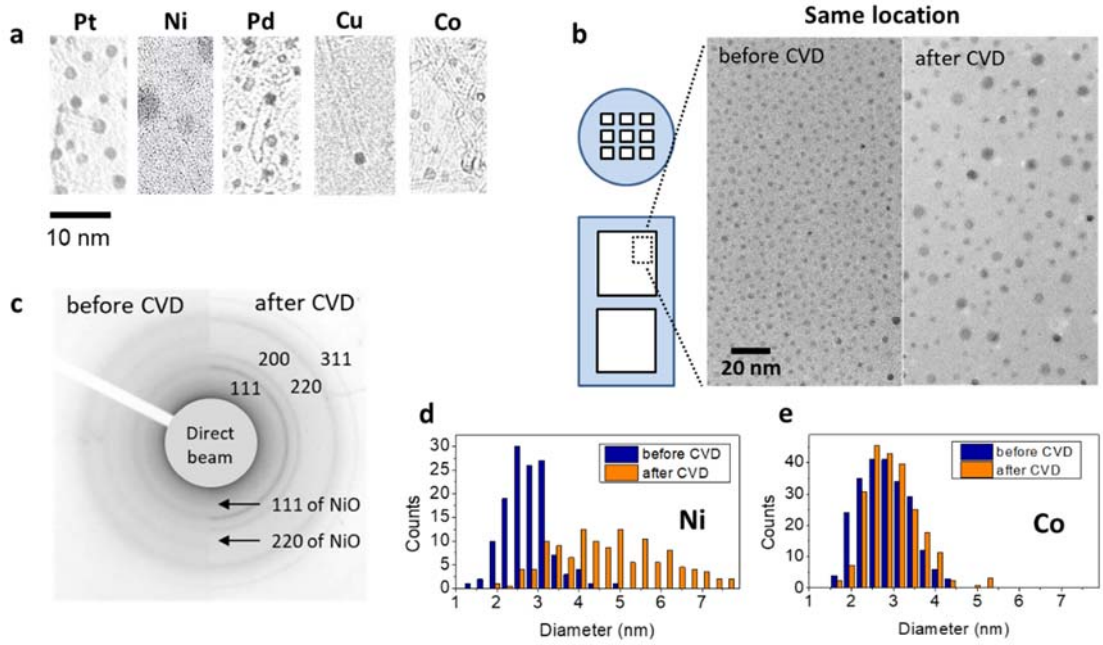

Figure 3 (a) TEM images of SWNTs synthesized from various mono-metallic particles sitting on a SiO_2 film; (b) a comparison of the exact same location of a Ni catalyst before and after a high temperature CVD; (c) corresponding SAED patterns of Ni catalyst; diameter distribution histogram of (d) Ni and (e) Co catalyst on SiO_2 before and after CVD, suggesting Ni deactivates due to the quick increase of particle size after carbon exposure.

One interesting phenomenon was observed for the case of Cu, in which the deactivation (in-efficiency) is due to metal loss. Cu is well-known for its efficient production of mono-layer graphene but is under debate as the catalyst for SWNT growth.[19] While in most cases Cu is not regarded as an efficient catalyst, some growth of very long SWNTs from Cu catalyst are also reported.[20] In our observations, one characteristic feature for Cu is many partial or complete hollow carbon spheres/nanotubes are observed (Figure 4a). This phenomenon is different from all other metals

investigated in this study. For Cu, there is little increase of particle size, but the particle density decreases by one order of magnitude after CVD. (Fig. S5) Even considering the diameter increase for individual particle, this result suggests a metal loss for Cu during the high temperature CVD. Figure 4b shows some enlarged images for such spheres and SWNTs. Some SWNTs are clearly observed but found to be closed at both ends.

The mechanism for the formation of such hollow SWNTs is mysterious but it is highly possible that the gradual loss of metal plays a dominant role. Previous calculation emphasized the importance of strong carbon-metal adhesion, and suggested catalyst may detach from a growing SWNT and generate hollow SWNTs.[21] However, from the tendency shown in Figure 4b, some catalytic particles have similar diameter with the spheres or short SWNTs attached, while many other particles are smaller than the size of the carbon structure. These particles are possibly the intermediate stage for the metal-losing particles. If being kept in the CVD for longer time, the particles may further shrink and end up in a fully hollow structure. Therefore, it is almost certain that gradual metal loss is responsible for the formation of hollow spheres and SWNTs. We believe the driving of such metal loss for Cu is thermal evaporation, which is also routinely observed in the synthesis of graphene.[22] Though there is possibility that metal atoms diffuse into the supporting SiO_2 film, evaporation is more likely after considering the relatively low boiling temperature of Cu than other metals in this study. Therefore, we claim evaporation-induced metal loss is a second mechanism that can directly observed by the current technique.

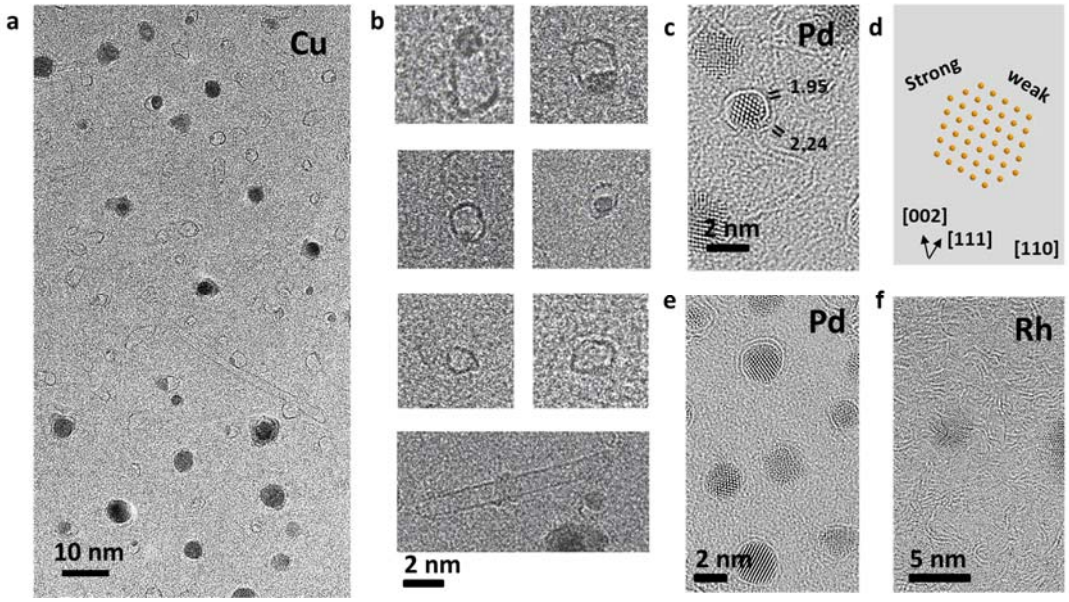

Figure 4 (a) A representative TEM image of Cu catalyst after CVD, showing many hollow mono-layer carbon spheres and SWNTs; (b) Enlarged TEM images reveal that some spheres and SWNTs are connected with a particle but many others are metal free; (c) a representative TEM image and

(d) corresponding crystal structure of Pd catalyst, clearly suggesting a facet dependent bonding of graphene layer; (e) a TEM image showing bilayer graphene coating occurs on many Pd particles; (f) a representative image of Rh particles, suggesting graphite layers precipitate everywhere and cover the whole substrate.

The third mechanism we demonstrate is inappropriate precipitation, which were observed for Pt, Pd, and Rh. Different from the previous two cases that catalyst particles expand (e.g. Ni) or shrink (Cu), these novel particles are stable at maintaining their sizes even in a high temperature environment and after carbon deposition. (Fig. S6) The average particle size for Pt and Pd are about 2 nm and remain unchanged after CVD. Also, the particles dispersed on the SiO_2 film at a much higher density (over 10^4 per μm^2) than other metals. However, efficient growth SWNTs are not achieved on these metals. As shown in Figure 4c-d, in all cases 1-2 layers of graphene can be observed on these metal particles, suggesting decomposition of carbon source into solid carbon efficiently occurs. But difficulties in the precipitation of these carbon atoms into tubular structure exists and seems to be responsible for the in-efficiency. The mechanism slightly differs for Rh and Pd. For the former, many random carbon flakes are produced from a Rh particle, suggesting that the interaction between graphene layers and Rh metals could be very weak. This results in a random and isotropic precipitation of carbon into all directions, as shown in Fig. 4f.

In the latter case, however, the graphene seems to have a much stronger interaction with metal surface, which makes it difficult for carbon atoms to precipitate into a SWNT. Figure 4c is a representative atomic resolution image of 2 nm Pd particle viewing from [110] direction. Clearly graphene-metal interspacing on different facets can be distinguished. The facet dependent growth of SWNT has been discussed since early time,[23, 24] but unfortunately there were very limited experimental evidence,[25-27] particularly on SWNTs. In our case, the image clearly reveals the difference among facets. As shown in Figure 4c, the carbon atoms on (002) are more firmly attached to Pd, while on (111) or (1-11), the carbon atoms are further from the surface (atomic structural scheme shown in Fig. 4d). But even on (111), the atoms only lift for a few angstrom up the surface and fail to form an efficient cap for a continuous growth of SWNTs. From this observation, Pd's problem lies in its in-efficient precipitation of tubular carbon even on the low energy (111) facet, which could possibly due to the too strong bonding between carbon and Pd. Similar phenomena were observed for Pt, which produces only short SWNTs. If somehow activated, Pt, Pd may be effective for producing small-diameter and high-density SWNTs arrays, as their number density is highest among all the metals investigated in this study. In addition, Pd shows the potential to produce double walled CNT, as many Pd particles are wrapped with two layers of graphene. We did not present elemental analysis in this report as all catalyst are monometallic, but energy-dispersive X-ray spectroscopy (EDS) and electron energy loss spectroscopy (EELS) also work on our grid. Therefore,

this technique is also applicable to bimetallic and other more complicated catalyst. [28]

4. Conclusions

In summary, we presented a TEM approach that metal catalyst deposition, and CVD synthesis of SWNTs can be performed on a MEMS fabricated thin SiO_2 film. Nano-sized particles and SWNTs grown from these particles can be imaged in their original morphology and in a statistical manner. Monometallic catalyst is used there as an example. Their behaviors before and after CVD are systematically re-visited by this new technique. Monometallic Co produces SWNTs efficiently following a tangential growth mode, while other metals are classified into three different deactivation/inefficiency mechanism: carbon induced size growth, evaporation driven metal loss, and inappropriate precipitation. The first one is vaguely understood but not visualized before, and the latter two mechanism were not possible to observe by previous techniques. Though some additional techniques are needed to support/explain the phenomenon, we believe the strategy proposed here serves as a key to the complicated catalytic synthesis of SWNTs. This method is also extendable to bimetallic or more complicated particles, catalyst behaviors at high temperatures, or even other nano-scale 1D and 2D materials.

Data accessibility. This article has no additional data.

Authors' contributions. R. X. and S.M. conceived the idea and designed the experiments. R. X. carried out the experiments. R. X. and S.M. analyzed data and wrote the paper.

Competing interests. We declare we have no competing interests.

Funding. Part of this work was financially supported by JSPS KAKENHI Grant Numbers JP15H05760, JP25107002, JP17K06187, JP17K14601, the JSPS-NSFC bilateral joint research projects, the "Nanotechnology Platform" (project No. 12024046) of the Ministry of Education, Culture, Sports, Science and Technology (MEXT), Japan.

Acknowledgements. We acknowledge the assistance from A. Kumamoto, T. Ito and H. Tsunakawa on TEM operation.

Reference

1. Yang F, Wang X, Li MH, Liu XY, Zhao XL, Zhang DQ, Zhang Y, Yang J, Li Y. 2016 Templated Synthesis of Single-Walled Carbon Nanotubes with Specific Structure. *Accounts Chem Res* **49**, 606-615. (10.1021/acs.accounts.5b00485)

2. Dai HJ, Rinzler AG, Nikolaev P, Thess A, Colbert DT, Smalley RE. 1996 Single-wall nanotubes produced by metal-catalyzed disproportionation of carbon monoxide. *Chem Phys Lett* **260**, 471-475. (Doi 10.1016/0009-2614(96)00862-7)

3. Kong J, Cassell AM, Dai HJ. 1998 Chemical vapor deposition of methane for single-walled carbon nanotubes. *Chem Phys Lett* **292**, 567-574. (Doi 10.1016/S0009-2614(98)00745-3)

4. Takagi D, Homma Y, Hibino H, Suzuki S, Kobayashi Y. 2006 Single-walled carbon nanotube growth from highly activated metal nanoparticles. *Nano Lett* **6**, 2642-2645. (10.1021/nl061797g)

5. Takagi D, Hibino H, Suzuki S, Kobayashi Y, Homma Y. 2007 Carbon nanotube growth from semiconductor nanoparticles. *Nano Lett* **7**, 2272-2275. (10.1021/nl0708011)

6. Liu BL, Ren WC, Gao LB, Li SS, Pei SF, Liu C, Jiang CB, Cheng HM. 2009 Metal-Catalyst-Free Growth of Single-Walled Carbon Nanotubes. *J Am Chem Soc* **131**, 2082-+. (10.1021/ja8093907)

7. Yang F, Wang X, Zhang DQ, Yang J, Luo D, Xu ZW, Wei JK, Wang JQ, Xu Z, Peng F, Li XM, Li RM, Li YL, Li MH, Bai XD, Ding F, Li Y. 2014 Chirality-specific growth of single-walled carbon nanotubes on solid alloy catalysts. *Nature* **510**, 522-+. (10.1038/nature13434)

8. Zhang SC, Kang LX, Wang X, Tong LM, Yang LW, Wang ZQ, Qi K, Deng SB, Li QW, Bai XD, Ding F, Zhang J. 2017 Arrays of horizontal carbon nanotubes of controlled chirality grown using designed catalysts. *Nature* **543**, 234-+. (10.1038/nature21051)

9. An H, Kumamoto A, Takezaki H, Ohyama S, Qian Y, Inoue T, Ikuhara Y, Chiashi S, Xiang R, Maruyama S. 2016 Chirality specific and spatially uniform synthesis of single-walled carbon nanotubes from a sputtered Co-W bimetallic catalyst. *Nanoscale* **8**, 14523-14529. (10.1039/c6nr02749k)

10. Maruyama S, Kojima R, Miyauchi Y, Chiashi S, Kohno M. 2002 Low-temperature synthesis of high-purity single-walled carbon nanotubes from alcohol. *Chem Phys Lett* **360**, 229-234. (Doi 10.1016/S0009-2614(02)00838-2)

11. Alvarez WE, Kitiyanan B, Borgna A, Resasco DE. 2001 Synergism of Co and Mo in the catalytic production of single-wall carbon nanotubes by decomposition of CO. *Carbon* **39**, 547-558. (Doi 10.1016/S0008-6223(00)00173-1)

12. Hata K, Futaba DN, Mizuno K, Namai T, Yumura M, Iijima S. 2004 Water-Assisted Highly Efficient Synthesis of Impurity-Free Single-Walled Carbon Nanotubes. *Science* **306**, 1362-1364. (10.1126/science.1104962)

13. Yoo CS, Soderlind P, Cynn H. 1998 The phase diagram of cobalt at high pressure and temperature: the stability of gamma(fcc)-cobalt and new epsilon '(dhcp)-cobalt. *J Phys-Condens Mat* **10**, L311-L318.

(Doi 10.1088/0953-8984/10/20/001)
14. Balbuena PB, Zhao J, Huang SP, Wang YX, Sakulchaicharoen N, Resasco DE. 2006 Role of the catalyst in the growth of single-wall carbon nanotubes. *J Nanosci Nanotechno* **6**, 1247-1258. (10.1166/jnn.2006.141)
15. Mchenry ME, Majetich SA, Artman JO, Degraef M, Staley SW. 1994 Superparamagnetism in Carbon-Coated Co Particles Produced by the Kratschmer Carbon-Arc Process. *Phys Rev B* **49**, 11358-11363. (DOI 10.1103/PhysRevB.49.11358)
16. Xiang R, Yang Z, Zhang Q, Luo GH, Qian WZ, Wei F, Kadowaki M, Einarsson E, Maruyama S. 2008 Growth deceleration of vertically aligned carbon nanotube arrays: Catalyst deactivation or feedstock diffusion controlled? *J Phys Chem C* **112**, 4892-4896. (10.1021/jp710730x)
17. Fiawoo MFC, Bonnot AM, Amara H, Bichara C, Thibault-Penisson J, Loiseau A. 2012 Evidence of Correlation between Catalyst Particles and the Single-Wall Carbon Nanotube Diameter: A First Step towards Chirality Control. *Phys Rev Lett* **108**. (ARTN 195503
10.1103/PhysRevLett.108.195503)
18. Aguiar-Hualde J, Magnin Y, Amara H, Bichara C. 2017 Probing the role of carbon solubility in transition metal catalyzing Single-Walled Carbon Nanotubes growth. *Carbon* **120**, 226-232. (10.1016/j.carbon.2017.05.035)
19. Li XS, Cai WW, An JH, Kim S, Nah J, Yang DX, Piner R, Velamakanni A, Jung I, Tutuc E, Banerjee SK, Colombo L, Ruoff RS. 2009 Large-Area Synthesis of High-Quality and Uniform Graphene Films on Copper Foils. *Science* **324**, 1312-1314. (10.1126/science.1171245)
20. Zhou WW, Han ZY, Wang JY, Zhang Y, Jin Z, Sun X, Zhang YW, Yan CH, Li Y. 2006 Copper catalyzing growth of single-walled carbon nanotubes on substrates. *Nano Lett* **6**, 2987-2990. (10.1021/nl061871v)
21. Ding F, Larsson P, Larsson JA, Ahuja R, Duan HM, Rosen A, Bolton K. 2008 The importance of strong carbon-metal adhesion for catalytic nucleation of single-walled carbon nanotubes. *Nano Lett* **8**, 463-468. (10.1021/nl072431m)
22. Chen X, Zhao P, Xiang R, Kim S, Cha J, Chiashi S, Maruyama S. 2015 Chemical vapor deposition growth of 5 mm hexagonal single-crystal graphene from ethanol. *Carbon* **94**, 810-815. (10.1016/j.carbon.2015.07.045)
23. Hong SL, Shin YH, Ihm J. 2002 Crystal shape of a nickel particle related to carbon nanotube growth. *Japanese Journal of Applied Physics Part 1-Regular Papers Short Notes & Review Papers* **41**, 6142-6144. (10.1143/Jjap.41.6142)
24. Hofmann S, Csanyi G, Ferrari AC, Payne MC, Robertson J. 2005 Surface diffusion: The low activation energy path for nanotube growth. *Phys Rev Lett* **95**. (ARTN 036101
10.1103/PhysRevLett.95.036101)
25. Zhu HW, Suenaga K, Hashimoto A, Urita K, Hata K, Iijima S. 2005 Atomic-resolution imaging of the nucleation points of single-walled carbon nanotubes. *Small* **1**, 1180-1183. (10.1002/smll.200500200)

26. Yoshida H, Takeda S, Uchiyama T, Kohno H, Homma Y. 2008 Atomic-scale in-situ observation of carbon nanotube growth from solid state iron carbide nanoparticles. *Nano Lett* **8**, 2082-2086. (10.1021/nl080452q)
27. Kohigashi Y, Yoshida H, Homma Y, Takeda S. 2014 Structurally inhomogeneous nanoparticulate catalysts in cobalt-catalyzed carbon nanotube growth. *Appl Phys Lett* **105**. (Artn 073108 10.1063/1.4893460)
28. Cui KH, Kumamoto A, Xiang R, An H, Wang B, Inoue T, Chiashi S, Ikuhara Y, Maruyama S. 2016 Synthesis of subnanometer-diameter vertically aligned single-walled carbon nanotubes with copper-anchored cobalt catalysts. *Nanoscale* **8**, 1608-1617. (10.1039/c5nr06007a)

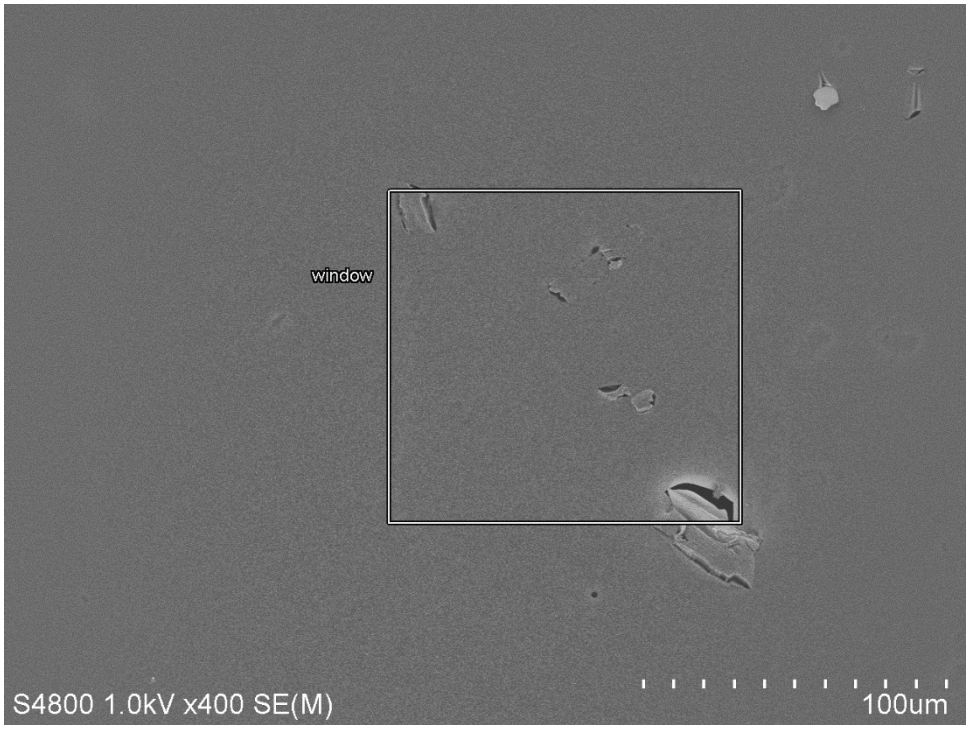

Figure S1 Original SEM image of SWNTs grown from Co catalyst on TEM grid (5 min growth), suggesting SWNTs grow efficiently and similarly on suspended SiO2 (window) region as the substrate region.

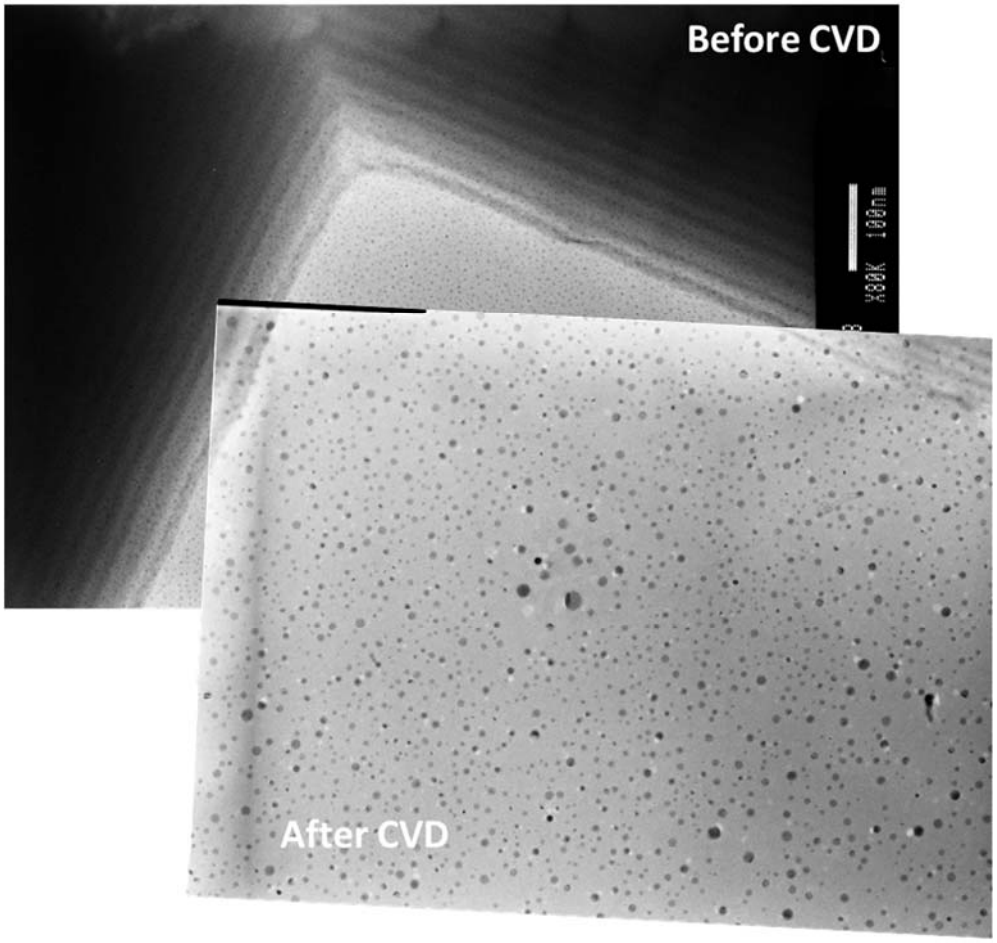

Figure S2 Original TEM images of Ni catalyst before and after growth, showing how images from the same location are obtained. To ensure a large viewing area, images are taken using film rather than CCD camera. Scans of the negative film are presented.

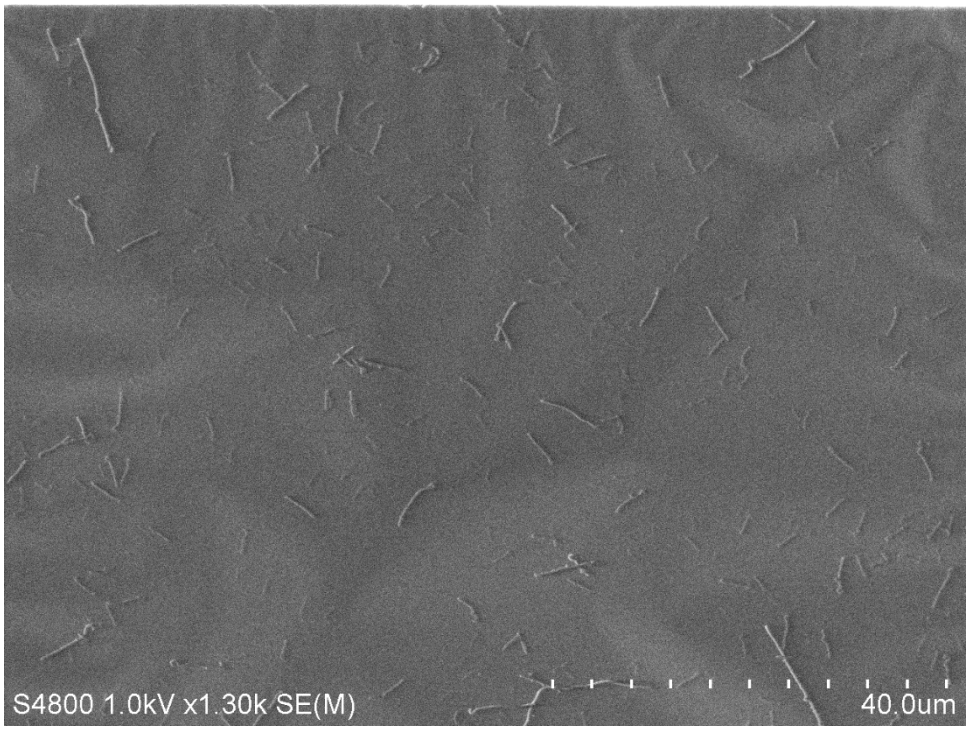

Figure S3 Original SEM image of SWNTs grown from Fe catalyst on suspended SiO2, showing long but only very sparse SWNTs can grow from monometallic Fe catalyst.

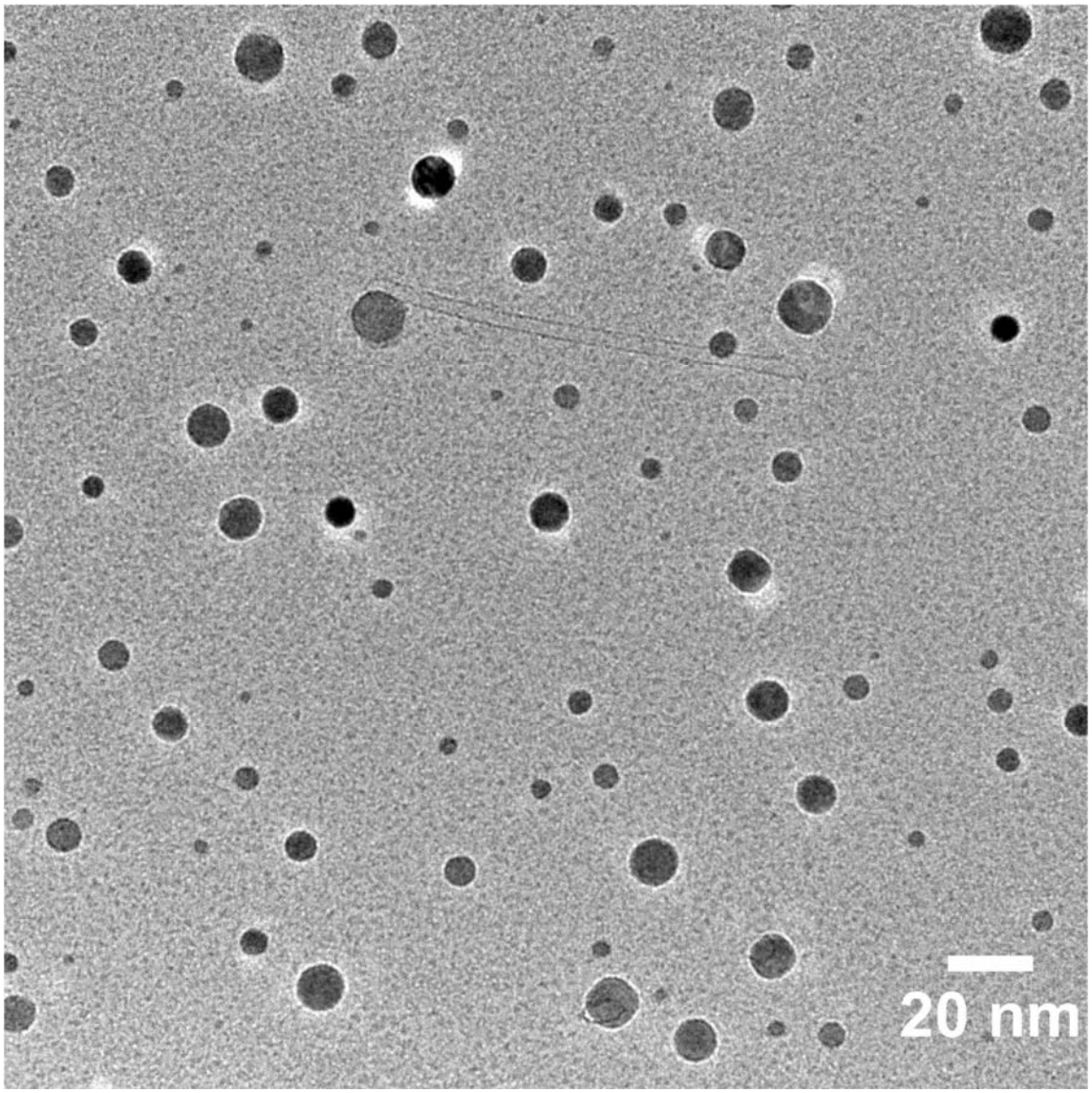

Figure S4 Original TEM image of SWNTs grown from Fe catalyst on suspended SiO2, showing the growth density is very small and SWNT diameter is smaller than catalyst, i.e., SWNTs follow a vertical growth mode.

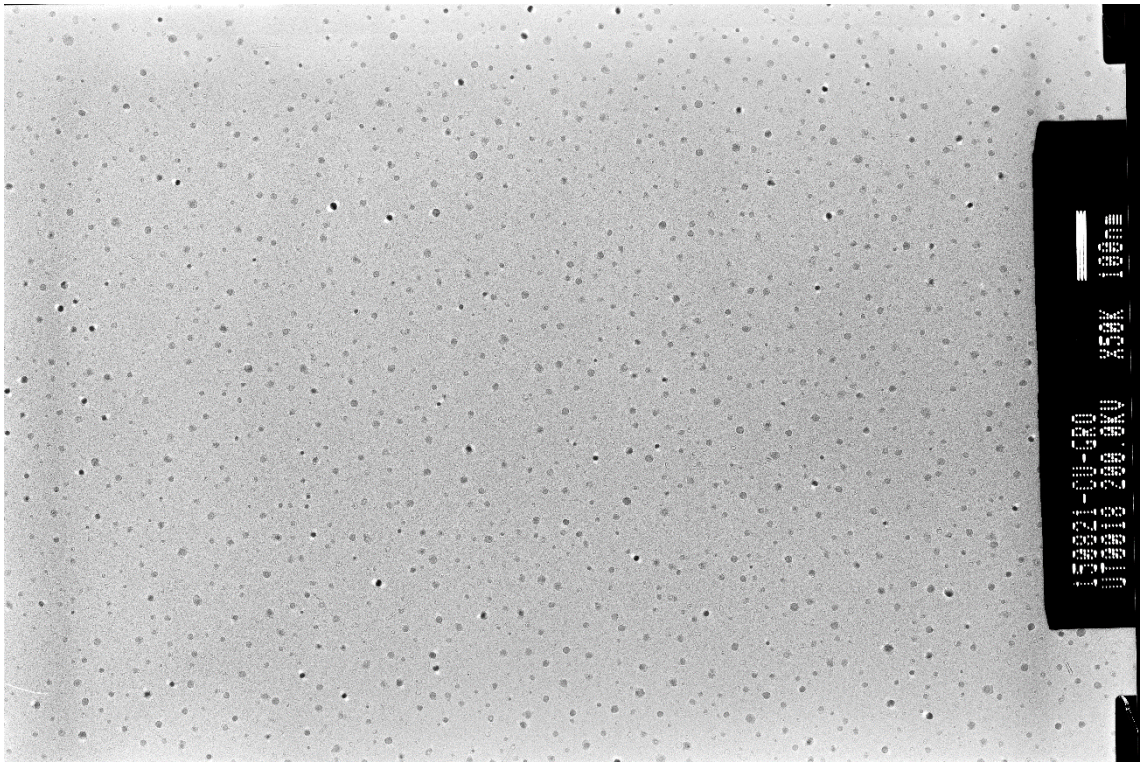

Figure S5 Original TEM images of Cu catalyst after SWNT growth, showing a very low catalyst density. Many hollow spheres and SWNTs can be uniformly observed on this grid. To ensure a large viewing area, images are taken using film rather than CCD camera. Scans of the negative film are presented.

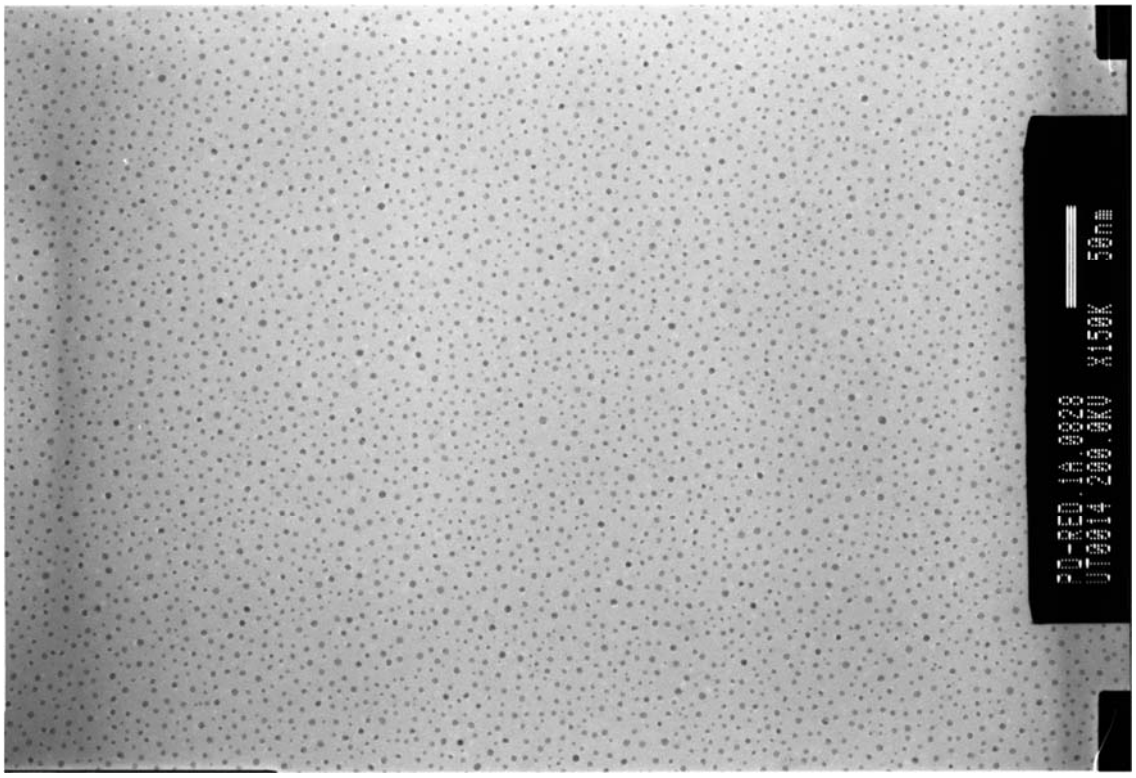

Figure S6 Original TEM images of Pd catalyst after reduction, showing a very high catalyst density. In comparison, the catalyst amount in Figure S5 is much less, which suggests that there is a significant loss of metal in case of Cu. To ensure a large viewing area, images are taken using film rather than CCD camera. Scans of the negative film are presented. The catalyst is extremely uniform on the entire grid.